Electrical Properties of Half Heusler Coatings Depending on Spray Process

Geoffrey Darut, Axel Portebois, Ludovic Vitu, Marie Pierre Planche, Hanlin Liao, Shantanu Misra, Christophe Candolfi, Bertrand Lenoir

Electrical Properties of Half Heusler coatings depending of spray process

Geoffrey DARUT, Axel PORTEBOIS, Ludovic VITU, Marie Pierre PLANCHE, Hanlin LIAO
UBFC, ICB-PMDM-LERMPS UMR6303, 90010 Belfort, France
corresponding authors, @: geoffrey.darut@utbm.fr

Shantanu MISRA, Christophe CANDOLFI, Bertrand LENOIR
Institut Jean Lamour, UMR 7198 CNRS – Université de Lorraine, 54011 Nancy, France

Abstract

Microstructure and physico-chemical properties of a thermally sprayed coating depend on the dynamics of the particles interacting with the spray jet. According to the process used (plasma, flame, etc.), porosity and phase composition could be different. This is especially the case for electrical properties. In this study, different spray processes (APS and HVOF) were investigated to spray Half Heusler powders type p and n. For that, the thermoelectric powder of Hf20Zr75Ti05CoSb80Sn20 (p-kind) and $Hf_{60}Zr_{40}NiSn_{98}Sb_{02}$ (n- kind) were selected due to their highly interesting electrical properties. The spray processes were evaluated through the measures of coating compositions and mechanical properties. A coating has only be get with plasma spray processes. The results revealed significant modifications in coating properties (atomic mass of elements, porosity) due to the operating parameters of plasma spray processes (F4MB or cascaded torch, plasma gas, etc.).

Introduction

The thermoelectric (TE) effect refers to phenomena by which either a temperature difference creates an electric potential or an electric potential creates a temperature difference [1][2]. Thermoelectric materials are used in thermoelectric systems for cooling or heating in sharp-range applications, and are being studied as a way to regenerate electricity from waste heat [3]. The efficiency of any TE material is evaluated by measuring the material's dimensionless figure of merit, ZT, defined by the following equation $ZT = S^2\sigma T/\kappa$, with S the Seebeck coefficient, σ the electrical conductivity, κ the total thermal conductivity, and T the absolute temperature in Kelvin [4]. Since S, σ, and κ depend all together upon the material properties, the main improvement obtained for ZT value has been achieved through the reduction of thermal conductivity from nano-structuring techniques. The rapid progress in this direction focused the efforts on the development of experimental methods and on the understanding of the phonons transportation to decrease thermal conductivity. The increase in ZT is not only a straight-forward matter of material choice but also involves smart design of material interfaces.

Global energy uncertainty with increasing energy demand triggers the search for high-efficiency energy conversion technologies. Thermoelectric devices can play a relevant role in energy collection and recovery. TE devices are 'fuel-free' solid-state devices with static parts and therefore are extremely reliable. In a non-thermal equilibrium environment, a non-negligible ratio of heat is lost meaninglessly. A solution consists in using TE devices to convert heat into electricity directly. Actually, this kind of elements are used in diverse applications, ranging from charging batteries to providing electricity for small devices in remote areas to powering deep-space vehicles [5].

The applications of TE device are still limited by their low conversion efficiency. According to the latest researches on TE materials, nanotechnology and advanced processes offer unprecedented opportunities in designing and fabricating complex material architectures with controlled microstructures [6]. The key factor to improve the performance of TE devices applications will steer developing the fine-structured TE materials. In this frame, it has been demonstrated that thermoelectric materials in sub-micro or nano-structure have the potential ability to improve the "figure of merit" (TE materials performance evaluation value) performance by 2 to 13 times over the value for bulk materials. To date, advanced low-dimensional nano or submicro-structured TE materials are not applicable for large-scale commercial applications because they are fabricated by atomic layer deposition processes such as molecular beam epitaxy. Using this technique, the manufacturing takes a rather long time, remains too expensive and leads to very strong restrictions in the amount of material to be produced. Moreover, they do not allow the design of flexible geometries [7] and the contacts with the heat source are always imperfect [8][9].

Thermal spraying is an additive manufacturing technique used in many industrial applications because of its high deposition rate (4kg/h), its high flexibility in terms of sprayable materials (metals, complex multi-component alloys, ceramics, ...), its thermal protection properties, the high possible coating thicknesses (from about 20 µm to several mm) and its low cost [10]. Although this technique offers new and unique ways of integration, it has so far received little attention from the TE community and deserves further investigation [11][12]. The main advantages of the thermoelectric generator manufactured by thermal spraying are:

- to create an intimate contact with the heat source and thus limit the parasitic contact thermal resistances;
- to provide thin or thick coatings of different materials and for multi functionalities (insulation or electrical conduction, energy conversion, …);
- to enable complex architectures that are not possible with current commercial TEGs;

- to be economical and scalable to facilitate a transfer to the industry. Actually, a lot of TE materials is developed according to the working temperatures, some of them are rather expensive and some are quite difficult to be manufactured. Conventional thermoelectric materials are Bi-Sb alloys, Pb-Te based materials and Si-Ge alloys [13]. Among the TE material families, Half-Heusler (HH) materials show high thermoelectric performances (ZT ~ 1.0 for both p and n-type materials) [14][15]. Half-Heusler compounds are characterized by an atomic ornamentation where a Ni atom is replaced by an ordered network of vacancies leading to compounds based on MNiSn or MCoSb (M = Zr, Hf, Ti). Their use as a thermoelectric module seems to be possible for the time being. Half-Heusler compounds offer several advantages [16][17]: i) n-type (based on TiNiSn or ZrNiSn) and p-type (based on TiNiSb) materials have good thermoelectric performance at moderate temperatures (400 - 900 K), ii) they are not very sensitive to oxidation and are thermally stable in a relatively high temperature range, iii) they are composed of low-cost elements compared to other commercially available TEs materials [16][18][19][20].

The aim of this project consists in studying the as sprayed coating feasibility of two Half Heusler materials, $Hf_{60}Zr_{40}NiSn_{98}Sb_{02}$ type n and $Hf_{20}Zr_{75}Ti_{05}CoSb_{80}Sn_{20}$ type p. The first study is devoted to HH type p material. The objective is to select the most appropriate thermal spraying process and identify the adequate operating parameters in order to obtain a coating as close as possible to the initial bulk material to guarantee the best thermoelectric properties.

Materials and processes

Feedstock

Half Heusler $Hf_{20}Zr_{75}Ti_{05}CoSb_{80}Sn_{20}$ (type-p) and $Hf_{60}Zr_{40}NiSn_{98}Sb_{02}$ (type-n) materials were received in the form of coarse bulks ranging in size from 5 to 50 millimeters, as shown in Figure 1.

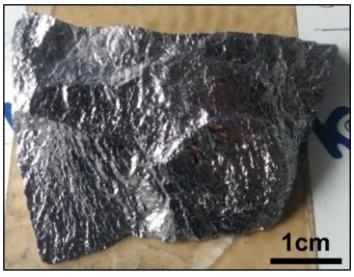

Figure 1: HH type p coarse bulks from Isabellenhütte Heusler GmbH & Co. KG, Dillenburg, Germany

The corresponding mechanical, thermal and electrical properties are exposed in Table 1.

Spray Process and Related Operating Parameters

Two plasma torches and a HVOF gun were successively used as thermal spraying processes during this study. The spraying kinematics were kept the same, i.e. a scanning of the substrate with a linear speed of 400 mm/s. A conventional plasma torch type F4MB (Oerlikon Metco, Switzerland) was first used with two set of spraying parameters. The diameter of the nozzle was 6 mm. The other operating parameters are shown in Table 2. The optimization of the coatings was further studied with a new generation of cascaded plasma torch: a Larmor 9 stages type configuration (Gulhfi AG, Wohlen, Switzerland) with a 8mm nozzle. Its architecture consists of a cathode and an anode segmented into 8 neutrodes. This so-called cascaded torch makes it possible to obtain higher voltages. Thus, it is possible to avoid or at least to reduce the use of hydrogen as a plasma forming gas. Consequently, plasma fluctuations are reduced leading then to reduce the defects in the coating microstructure. On the other hand, the positioning of the arc attachment at the exit of the plasma torch pushes it further outwards, allowing the particles to be injected into a much hotter medium compared to the conventional F4MB torch. The spray distance was 120mm. The HVOF process used in this study is an Egun (Flame Spray Technologies (Nederland). An oxygen and ethanol mixture composes the flame. The spraying distance was 300 mm.

Table 1: Mechanical, thermal and electrical properties of the two HH materials studied in the project.

		HH type-n	HH type-p
Electrical resistance [Ω.m]	**r1**	$-2.3.10^{-15}$	
	r2	$3.8.10^{-12}$	$-1.1.10^{-11}$
	r3	$1.5.10^{-9}$	$2.7.10^{-8}$
$Rho=r1*T^3+r2*T^2+r3*T+r4$	**r4**	$2.7.10^{-6}$	$-1.2.10^{-6}$
Seebeck coefficient [V/K]	**s1**	$4.7.10^{-14}$	
	s2	$6.0.10^{-11}$	$-2.4.10^{-10}$
	s3	$-2.5.10^{-7}$	$4.4.10^{-7}$
$S=s1*T^3+s2*T^2+s3*T+s4$	**s4**	$-2.6.10^{-5}$	$-7.7.10^{-6}$
Thermal conductivity [W/m.K]	**λ1**		
	λ2	$4.2.10^{-6}$	$1.5.10^{-6}$
	λ3	$-5.9.10^{-3}$	$-3.4.10^{-3}$
$\lambda=\lambda1*T^3+\lambda2*T^2+\lambda3*T+\lambda4$	**λ4**	6.9	5.5
Melting temperature [°C]		1510	
Elastic modulus [GPa]		183	194
Shear modulus [GPa]		80	79

Table 2: Plasma spray operating parameters.

Designation	F1	F2	C1	C2	C3	C4	C5	C6	C7	C8	C9
Powder [µm]	<40		17-57								
Plasma torch	F4-MB		Cascaded torch								
Ar/H_2 flow rate [SLPM]	60/6	45/11	95/0				80/0	60/0	40/0	95/0	70/0
Arc current intensity [A]	600		300	350	200	150	200				150
Power [kW]	37	43	29	35	16	11	16	15	13	17	11

Substrates were made of low carbon steel plate 50*20mm² and 1.6mm in thickness. Prior to spraying, surfaces to be covered were grit-blasted with F36 white corundum (α-Al_2O_3) particles of 250µm average diameter in order to achieve an average roughness (Ra) of about 4µm. Before spraying, they were degreased with ethanol.

Characterization Techniques

Microhardness of coatings was measured by a Vickers hardness tester (Leica VMHT30A, Germany) under a load of 300gf force applied for a dwell time of 15s. 8 random indentations were done on the polished cross section.

A field emission scanning electron microscope (FESEM JEOL 7800F, Japan) was used to observe powder and coating microstructures. The chemical compositions were determined by energy dispersive spectrometry (EDS, SDDX-Flash 6130, Bruker, Germany).

A X-ray diffractometer (XRD, D8 Advance, Bruker, Germany) equipped with CoKα radiation (λ = 0.179 nm) was used to determine the composition of the powder and coatings.

The particle size distribution was determined by a Mastersizer 2000 instrument (Malvern, UK).

Results

HH type p powder manufacturing and characterization

The characteristic dimension of a thermal spray powder is of the order of ten microns to 100 microns. Because of the very coarse size of the HH material blocks, it is necessary to initially crush them in order to be able to use them in a grinder afterwards. The first step was to reduce the size of these large blocks to fragments smaller than a centimeter, thus to perform a fine crushing. The crushing was carried out by means of a hydraulic press by placing the fragments between two bites. A sieving is done after each crush in such a way that the particles larger than a millimeter were filtered to grind them once again. Once all the fragments have been reduced, a grinding was carried out to obtain a granulometry lower than 80µm. The measured HH type-p microhardness was 829±40.6HV0.3. Due to this high hardness value, tungsten carbide grinding equipment is required. A PM400 (Retsch, Germany) planetary ball mill is used. Two grinding stations were employed. The grinding parameters were 125ml tungsten carbide jars, 20mm diameter tungsten carbide balls, a rotation speed of 400rpm and a cycle time of 30s. The Figure 2 shows the particle size distribution obtained after 1 cycle. On the plot of the particle size curve we still note many particles larger than 100µm. However, the grinding cycle has been kept at 30s to avoid the formation of very fine particles smaller than 10µm that could obstruct the powder transportation equipment during spraying. By extending the grinding cycle, the coarse particles would of course be reduced to particles smaller than 40 or 80µm, but at the same time the particles suitable for thermal spraying (between 10 and 80µm) would also be ground into much finer particles (yellow curve). The yield of particles suitable for thermal spraying processes would then be reduced. Therefore, it was preferable to link several cycles of 30s interspersed with sieving stages at 80µm in order to limit the formation of these very fine particles. The particles remaining in the sieve are ground again for an additional cycle.

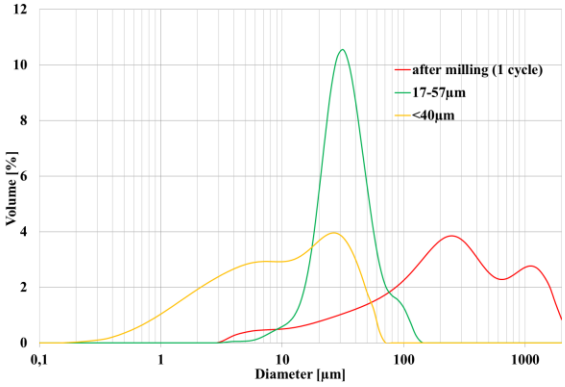

Figure 2: HH type p powder size distributions after the successive operations for reducing the size

Following these steps of powder preparation, different average size distributions were finally obtained using a 40µm sieving grid. To obtain the appropriated inferior size distribution of the powder, an elutriator was employed. The following grain sizes were therefore obtained: -40µm, 40-80µm and 17-57µm (Fig. 2). It should be noted that during the various parametric grinding tests, especially the first moments of the grinding process, many very fine particles smaller than 10 microns are generated. Despite the modification of the mill rotation speed and the size and number of grinding balls used, the generation of these very fine particles, inappropriate for thermal spraying, was unavoidable.

Figures 3 and 4 show the microstructures of the initial bulk and the resulting powder obtained after crushing and grinding. The bulk has a dense microstructure with a randomly scattered porosity. The powder, on the other hand, is angular. The first important point to check is the preservation of the composition between the initial fragment of several centimeters and the powder obtained. The chemical analysis of the elements in atomic concentration was carried out by EDS. The main elements of the HH material are identified: namely cobalt, hafnium, zirconium, antimony, tin and titanium. The mapping of the elements within the microstructure of the bulk and the powder shows a homogeneous mixture without the presence of a distinct zone richer in the atomic concentration of a particular chemical element (see Fig. 5 and 6). The different atomic proportions of the elements are shown in Table 3. After grinding, there is a decrease of the Sb and Zr (-6% at.) elements to the benefit of the appearance of the oxygen (6% at.).

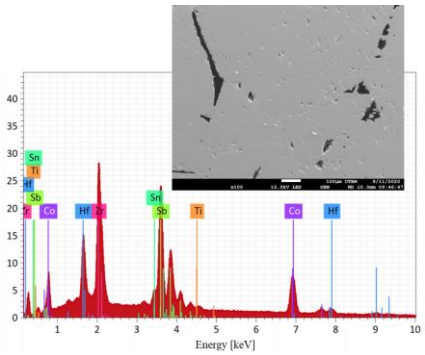

Figure 3: EDS analysis of HH type p bulk microstructure and elements

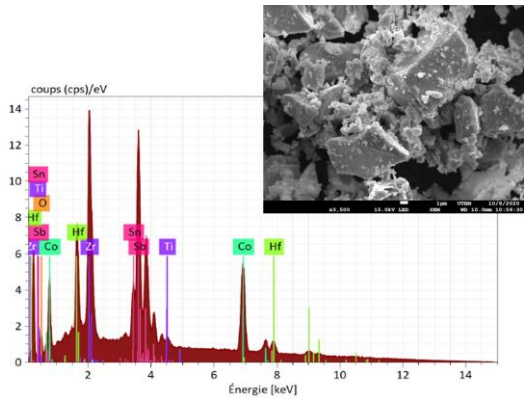

Figure 4: EDS analysis of HH type p milled powder morphology and element

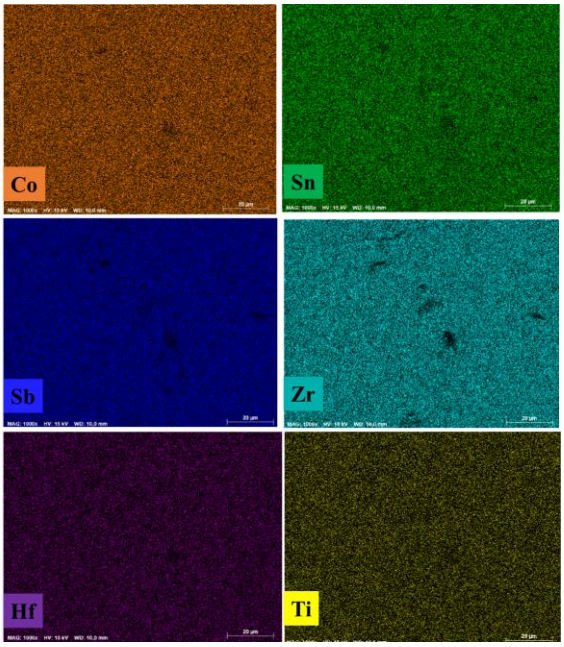

Figure 5: Chemical cartography of HH type p bulk element

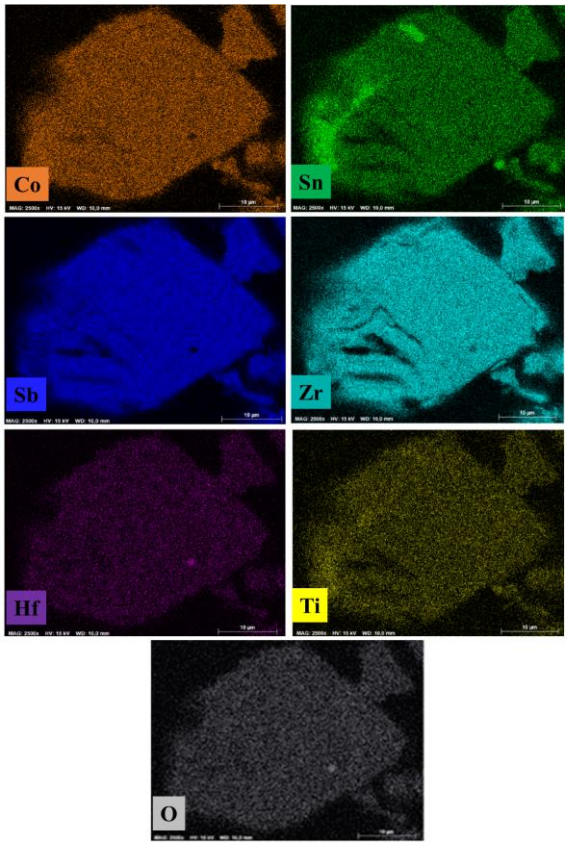

Figure 6: Chemical cartography of HH type p powder element after milling

Table 3: HH type-p bulk, powder and coatings composition (%at.) and porosity (%)

	%at.							porosity
	Co	**Hf**	**Sn**	**Sb**	**Zr**	**Ti**	**O**	**%**
HH type p bulk	33,6	6.8	3.1	30.8	24.8	0.9	0	
HH type p powder	35.5	7.3	5.8	24.5	18.8	1.3	6.8	
E1	20.0	9.1	1.9	4.2	30.0	1.8	33.2	0.8
F1 (60/6-600)	20	9.1	1.9	4.2	30	1.8	33.2	4.4
F2 (45/11-600)	20	10	2	5.9	27.8	2	32.2	3.3
C1 (95-300)	30	6.1	5.5	19	22	1.9	15.4	4.1
C2 (95-350)	29.1	6.3	4.5	17.8	21	1.5	19.7	3.2
C3 (95-200)	29.8	5.9	6.2	19.7	20.4	1.9	16	7.7
C4 (95-150)	29.6	6.5	5.5	22.6	19	1.6	15	13.5
C5 (80-200)	30.1	6.1	6.1	20.3	20.4	1.6	15.2	9.7
C6 (60-200)	31.3	6.4	6.5	20.6	21.9	1.8	11.3	8.5
C7 (40-200)	28.6	6.7	4.6	17.7	21.4	1.7	19.2	8.8
C8 (95-200)	29.8	6	6.8	21.1	20	1.7	14.5	10.1
C9 (70-150)	30.6	6	5.9	22.5	20.7	1.5	12.7	17

The grinding was carried out under atmosphere, which may explain first the reaction of the air with the fragments and particles generated. Second, during the rotation, the impacts/bearings of the balls generate heat which leads also to oxidation. The X-ray diffraction patterns of the bulk and powder are displayed in Figure 7. The predominant phase is CoSbZr.

HVOF experiment

As mentioned previously, the hardness of this HH material is relatively high. However, the HVOF process has nevertheless been studied because of the characteristics it can bring in terms of in-flight particles based on a relative high-velocity and medium temperature. Indeed, this process is relatively well adapted for nickel or cobalt base materials. The objective here is to preserve the composition of the powder resulting from the crushing and grinding stages of the initial bulk. A first test was conducted with the finest -40µm powder and the operating parameters (E1) of 518L/min of oxygen and 23.8L/h of ethanol (low temperature flame for Egun). After several seconds, the pipe between the powder feeder and the injectors was clogged. The resulting coating is shown in Figure 8. The coating is relatively dense. The chemical analysis is reported in Table 3 and compared in Figure 9 (brown curve) with bulk, powder and plasma coatings.

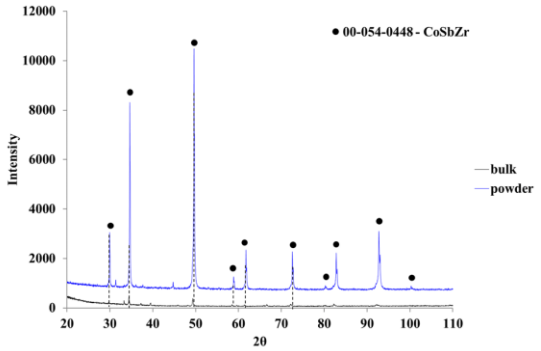

Figure 7: X-ray diffraction pattern of HH type-p bulk and final powder

Compared to powder, the atomic concentration of the elements Co, Sn, Sb decreases strongly and the element zirconium becomes majority. In spite of a low energy and high-speed flame setting, the oxidation is important with an oxygen concentration which passes from 6 to 33%. The small powder particle size lower than 40µm can also explain such a high rate. Figure 10 shows the distribution of the elements in the coating. It indicates some common areas of depletion for Co, Hf and Ti elements. Instead, the Sn element predominates. A larger grain size of 17-57µm was also tested to prevent clogging. Different spraying parameters have been studied by sweeping a whole range of flame energy from a fast and cold flame (560L/min of oxygen and 26L/h of ethanol) to a slow and hot flame (410L/min of oxygen and 28.5L/h of ethanol). No clogging occurs. Despite numerous spraying tests, it was not possible to obtain a sufficiently thick coating (higher than 10 µm). due to the bouncing of many particles on the substrate surface. This means that the energy available in the ethanol-based HVOF process is insufficient to treat HH material even if the dimensions of the powder are close to the standards of the HVOF process. The use of another HVOF process with a more energetic flame using kerosene as fuel such as JP-5000 could be a solution to melt this material.

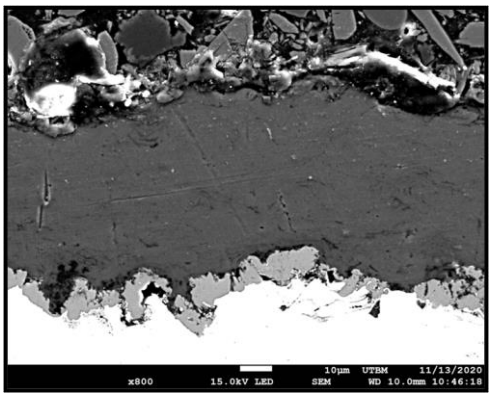

Figure 8: Microstructure of E1 coating get by HVOF

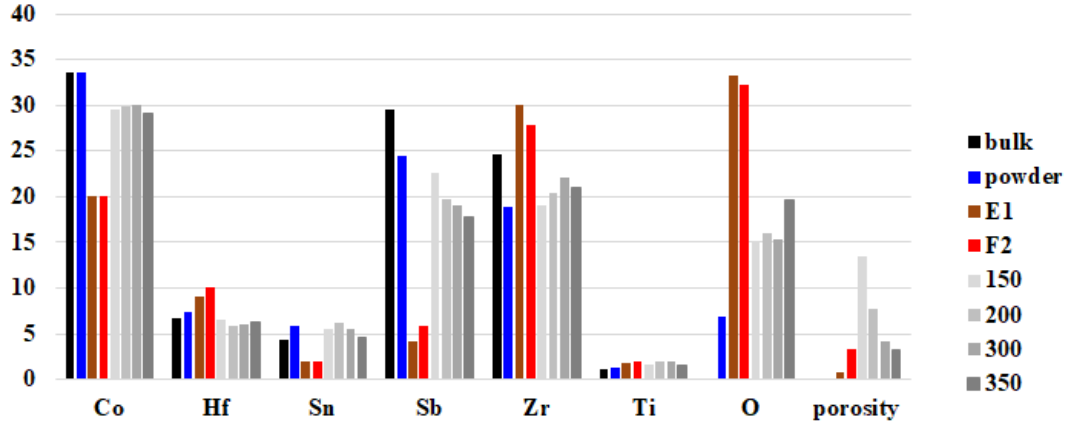

Figure 9: HH type-p coatings composition (%at.) and porosity (%):E1 (HVOF), F2 (F4MB) and cascaded plasma torch with a 95L/min Ar plasma jet for different arc current intensities from 150 to 350A – comparison with the bulk and powder

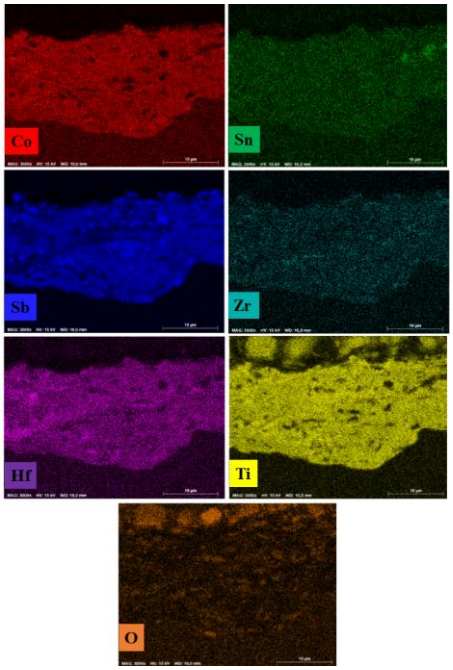

Figure 10: Element chemical cartography of E1 coating get by HVOF

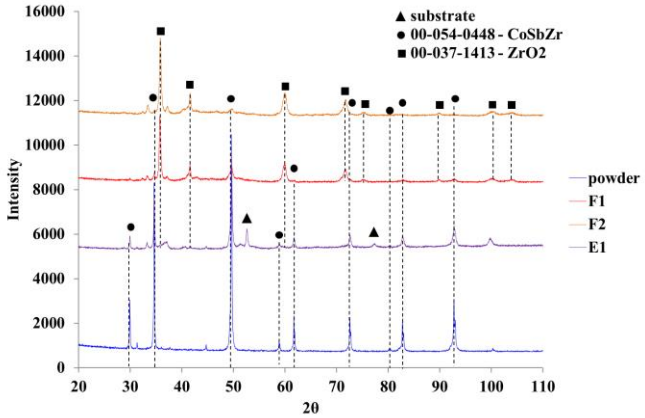

Figure 11: X-ray diffraction pattern of HH type-p coatings by F4MB plasma torch (F1, F2) and Egun (E1)

X-ray diffraction analysis of the small coating shows a very good correlation with the phase of the powder. The CoSbZr diffraction peak is preserved. The use of the very fine material with the HVOF process is very promising. However, the duality between nozzle clogging for the fine particles and high hardness and low deformation of the larger particles makes optimization complex.

F4MB plasma torch

Due to the difficulties to obtain a coating composed of HH material, a conventional plasma torch type F4MB was used. The available energy should be high enough to melt the HH material properly for a grain size lower than 80µm. With plasma spray technology, the objective will be to find the right operating parameters so as not to over-oxidize the material while melting it correctly in order to limit the presence of defects within the microstructure. Table 2 shows the two spraying parameters that were used: a 60/6 (F1) and 40/11

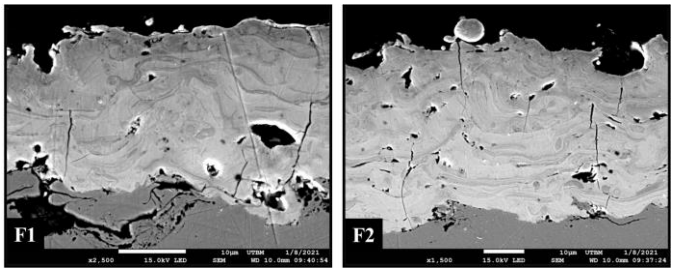

Figure 12: F1 and F2 coating microstructures get by F4MB torch plasma spraying

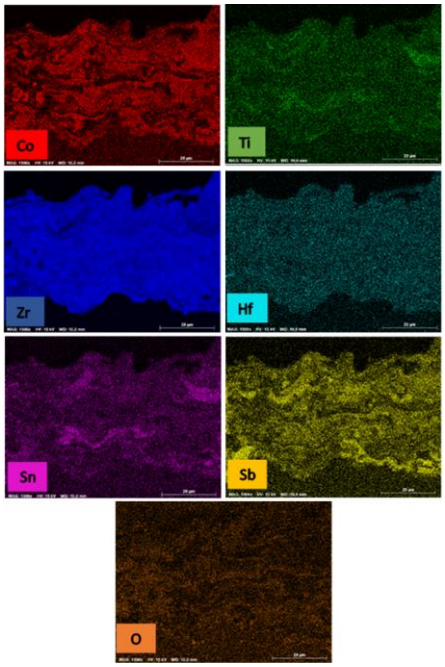

Figure 13: Element chemical cartography of F1 coating get by F4MB plasma torch

(F2) argon/hydrogen plasma. The aim of these two tests is to have an overview of the feasibility of using such plasma torch with the guarantee to respect the initial composition of the powder while obtaining the densest possible coating. The microstructures of the coatings F1 and F2 are shown in Figure 12. It shows a lamellar microstructure with different contrasts which indicates a probable strong oxidation of the material. Porosity is also observed, which indicates that not all the particles have been treated correctly within the plasma, probably due to the presence of jet fluctuations linked to the use of diatomic hydrogen gas. The porosity is of the order of 4%. The atomic concentrations of the elements are given in Table 3. The composition is globally similar between the two spraying parameters tested, i.e. a hot, slow plasma versus a cooler, faster plasma. The composition of the F2 coating is shown in Figure 9 in order to compare it with that of the initial powder. As with the HVOF process, there is a strong decrease in the following elements cobalt, tin and antimony. The oxygen element also increases considerably. The analysis of the distribution of the different chemical elements shows a preferential location of elements with others (cf. Fig. 13). We note the grouping of the element tin with titanium, cobalt with antimony, zirconium with oxygen. The element hafnium is

homogeneously distributed. There is therefore a significant upheaval in the initial elemental distribution of the powder.
X-ray diffraction analysis of the coatings shows a significant change in the phase composition of the material. The initial peaks of the CoSbZr powder almost disappear. A significant amount of zirconium oxide ZrO_2 is formed during the spraying process. Under these conditions, the F4MB torch coupled with this set of parameters is not suitable for the spraying of this material. This study did not involve further exploration of operating parameters with the F4MB torch in order to focus on the potential of new generations of so-called cascaded plasma torches.

Cascaded plasma torch

The use of a cascade plasma torch aims to avoid voltage fluctuations by stabilizing the electric arc at the nozzle exit by the presence of neutrodes in the design of this torch. The overall length of the anode is increased compared to a conventional F4MB torch. The result is a higher arc voltage which, in turn increases the power of the plasma. A lower arc current is required without likely the use of hydrogen gas. That is why the parametric study that has been carried out aims at using a hydrogen-free plasma and adapting the energy of the plasma by varying the argon flow rate and the intensity of the arc current.
Different spraying conditions were tested in order to obtain an initial view of the microstructure and composition of the coatings that could be obtained. The spraying parameters are presented in Table 2. Different argon flow rates from 40 to 95L/min and arc current intensities from 150 to 350A were tested. The carrier gas flow rate was adjusted according the parameter set used. The resulting microstructure of the coatings is shown in Figure 14. The atomic concentrations of the elements are listed in Table 3 and reported in Figure 9 and 15 to better note the evolution of the compositions as a function of the varying spraying parameters. The observation of the microstructures shows that the highest porosity (13.5 to 17%) is obtained for a low arc current intensity of 150A and a high plasma gas flow rate of 70 or 95L/min. The plasma has a low energy with a very fast flow velocity. This results in a low residence time of the particles within the plasma limiting their melting. Porosity defects are therefore found within the microstructure. This confirms the observations made with the HVOF process with the incompatibility of a good heat treatment of the particles in a fast and low energy jet. At a constant plasma gas flow rate (95L/min), the increase in arc current intensity leads to a decrease in the porosity within the coating. The plasma becomes more and more energetic allowing the treatment of a larger number of particles that arrive in a molten state at the surface of the substrate. In terms of the evolution of the atomic concentrations of the elements, the increase in plasma energy increases the oxidation of the coating and the decrease of the elements tin and antimony. Cobalt, hafnium, zirconium and titanium elements have proportions that remain relatively stable. Compared to coatings obtained by HVOF and conventional plasma processes with the F4MB torch, the amount of oxidation is greatly reduced. Cobalt, antimony, hafnium, tin elements are retained to a greater extent in the coatings. However, the porosity is higher. These elements can be explained by the change in plasma configuration with the use of a so-called cascaded plasma torch. The configuration of this torch involves several modifications compared to a F4MB torch. First of all, maintaining the arc attachment at the last stage of the cascaded torch implies a plasma pushed further outside the torch. Less energy is dissipated in the cooling circuit and therefore more energy is available for particle treatment. Conversely, the plasma gas flow rate is higher, reducing the

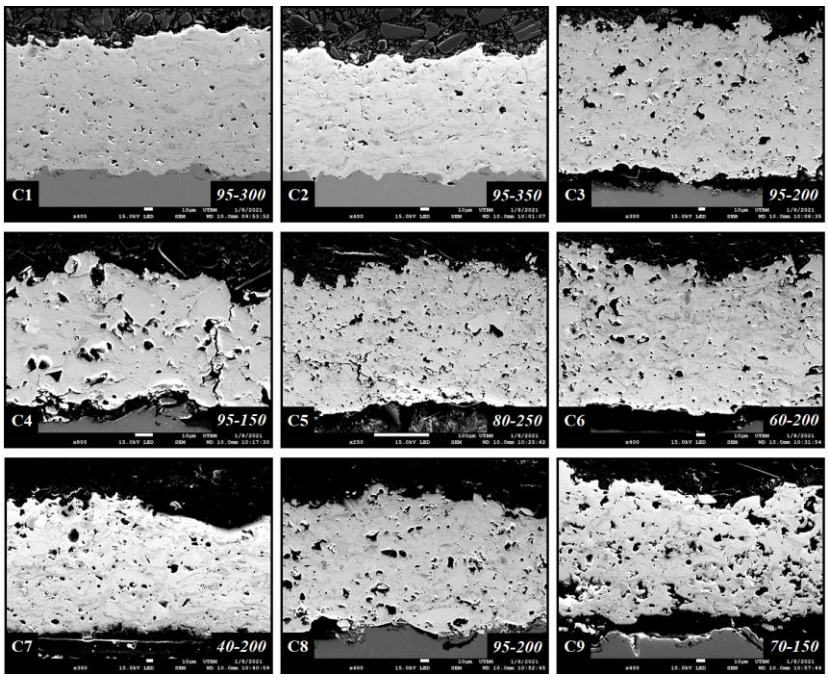

Figure 14: Coating microstructures get by cascaded plasma torch (Ar flow rate in l/min – Arc current intensity in A)

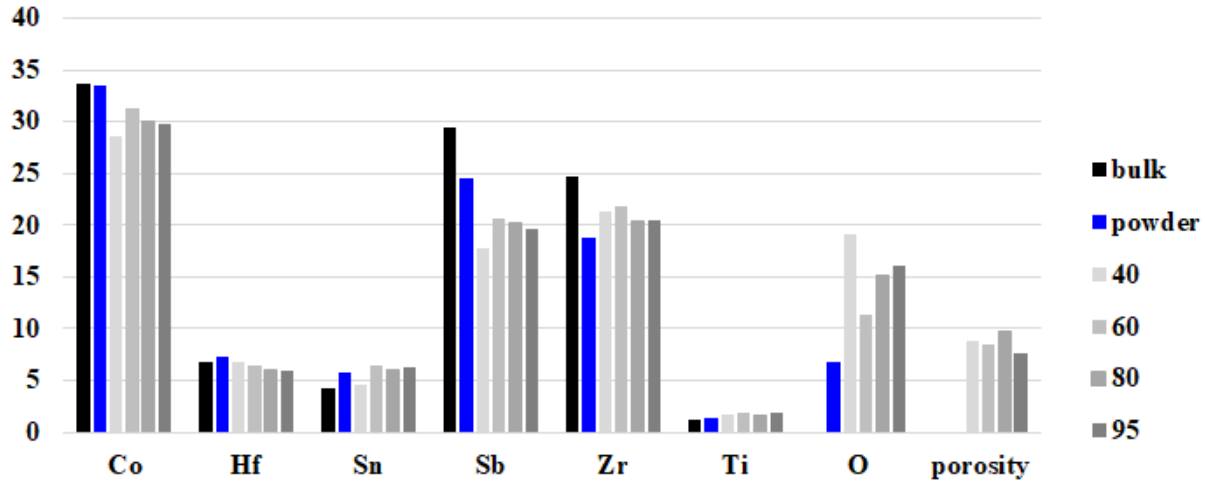

Figure 15: HH type-p coatings composition (%at.) and porosity (%) for the cascaded plasma torch with a 200A arc current intensity for Ar plasma gas flow rates from 40 to 95l/min – comparison with the bulk and powder

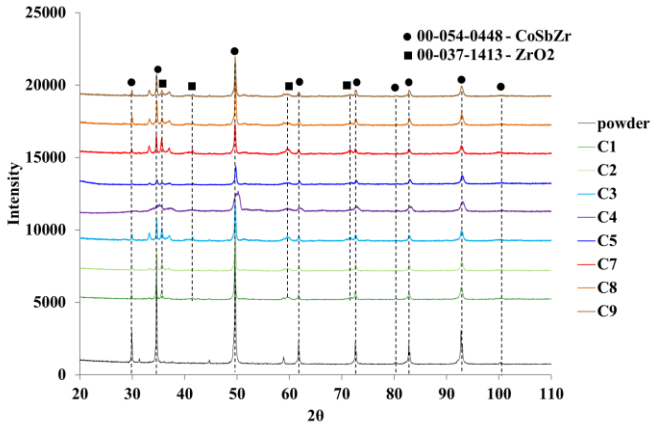

Figure 16: X-ray diffraction pattern of HH type-p coatings by cascaded plasma torch

residence time of the particles. Also, the nozzle diameter is 8mm instead of the 6mm of the F4MB torch, which tends to reduce the gas flow velocity. All these main differences lead to changes in the composition of the coatings. The X-ray diffraction spectra show a best phase conservation with the cascade torch (cf. Fig. 16). Depending on the parameters, a more or less important zirconium oxide composition emerges. For the same arc current intensity of 200A, increasing the argon flow rate from 40 to 95L/min greatly reduces the intensity of the ZrO_2 peak. More in-depth diagnostic studies must be carried out in order to better understand the effects of the various parameters (number of neutrodes, anode length, nozzle diameter, hydrogen, etc.) of this new design of plasma torch in order to guarantee a sufficient melting of the particles while avoiding the formation of zirconium oxide.

The influence of the plasma gas flow rate at a constant arc current intensity of 200A was studied. There is no noticeable influence on the porosity of the coatings in the range of parameters tested. The atomic concentrations of the individual elements vary slightly without any trend being discernable. This could be mean that the particle velocity generated by the increased plasma gas flow velocity does not have a pronounced influence on the coating composition compared to arc current intensity modification.

Conclusions

This study consisted in studying the feasibility of spraying a Half Heusler type-p material of composition $Hf_{20}Zr_{75}Ti_{05}CoSb_{80}Sn_{20}$ by HVOF and plasma spraying. The first part showed the possibility of manufacturing a powder that can be used in thermal spraying from an initial material in bulk form. The different successive crushing and grinding steps do not significantly alter the atomic concentration of the various elements of the final powder and their distribution in the particles. Slight oxidation is nevertheless present due to the mechanical actions under atmosphere.

The use of HVOF process has shown a difficulty to obtain a coating. Only a very fine powder < 40µm allows its complete melting within the thermal jet. However, a problem of clogging of the powder in pipe appeared. The use of larger particle sizes 40-80µm and 15-57µm did not result in a coating manufacturing in the parametric range of the process. The coating resulting from the spraying of the fine powder is relatively dense, but a majority phase of zirconium oxide ZrO_2 phase is formed to the detriment of the CoSbZr initial phase of the powder.

The use of plasma processes has made it possible to obtain coatings from a powder with a particle size of 15-57µm. The use of a F4MB plasma torch generates highly oxidized coatings with a decrease in the atomic concentrations of the following elements antimony, tin and cobalt. These phenomena are considerably reduced by using a so-called cascaded plasma torch. Despite the non-optimized couple of spraying parameters, the elemental composition of the coatings is closer to the initial powder. Following these initial spraying tests, an optimization of the compositions is still possible by modifying the spray distance or the configuration of the cascaded torch. Indeed, it is possible to extend or reduce the length of the segmented anode by adding or removing neutrodes. Also, the addition of a small amount of hydrogen can be studied while limiting voltage fluctuations.

Acknowledgments

The participants in this project would like to thank IRT-M2P French institute for their financial support and Pr Omar EL KEDIM and his phD student Yuchen LIU for their assistance in the HH powder preparation.

References

[1] T. J. Seebeck, *Abhandlungen der Deutschen Akademieder Wissenschafren zu Berlin*, Vol. 265 (1823)

[2] J.C. Peltier, *Ann. Chim. Phys*. Vol. 56 (1834), p.371

[3] C. Barreteau, Matériaux céramiques thermoélectriques pour la production d'électricité propre, Thesis, Université Paris Sud - Paris XI, 2013. in french. ffNNT : 2013PA112167ff. fftel-00876611

[4] G. Roelkens, *et al.*, "III-V/Si photonics by die-to-wafer bonding", *Mater. Today*, Vol. 10, No. 7-8 (2007), p. 36-43 https://doi.org/10.1016/S1369-7021(12)70178-5

[5] G .D. Mahan et al.," Thermoelectric Materials: New Approaches to an Old Problem", *Physics Today*, Vol. 50 (1997), p. 42 https://doi.org/10.1063/1.881752

[6] O. H. Ando Junior, *et al.*, "A review of the development and applications of thermoelectric microgenerators for energy harvesting", *Renew. Sust. Energ. Rev.*, Vol. 91 (2018), p. 376-393 https://doi.org/10.1016/j.rser.2018.03.052

[7] S. Leblanc, *et al.*, " Material and manufacturing cost considerations for thermoelectrics", *Renew. Sust. Energ. Rev.* Vol. 32 (2014), p. 313-327 http://dx.doi.org/10.1016/j.rser.2013.12.030

[8] C. Kim, *et al.*, " Development of a numerical method for the performance analysis of thermoelectric generators with thermal and electric contact resistance", *Applied Thermal Eng*. Vol. 130 (2018), p. 408-417 https://doi.org/10.1016/j.applthermaleng.2017.10.158

[9] T. Kim et al, " Direct contact thermoelectric generator (DCTEG): A concept for removing the contact resistance between thermoelectric modules and heat source", *Energy Conversion and Management*, Vol. 142 (2017),p. 20-27 https://doi.org/10.1016/j.enconman.2017.03.041

[10] A. Vardelle, *et al.*, "The 2016 thermal spray roadmap", J. *Therm. Spray Technol.* Vol. 25, No. 8 (2016), p. 1376-1440 https://doi.org/10.1007/s11666-016-0473-x

[11] J. Schilz, *et al*., "On the Thermoelectric Performance of Plasma Spray-formed Iron Disilicide", *Mater. Sci. Lett*., Vol. 17 (1998), p. 1487-1490 https://doi.org/10.1023/A:1026486703748

[12] M. Tewolde, *et al.*, "Thermoelectric Device Fabrication Using Thermal Spray and Laser Micromachining", J. *Thermal Spray Technol. Vol.* 25, No. 3 (2016), p. 431-440 https://doi.org/10.1007/s11666-015-0351-y

[13] S. Mesra, Towards highly-efficient telluride-based thermoelectric materials, Thesis, Institut Jean Lamour, Nancy. 2013. in french

[14] T. Zhu, *et al.*, "High Efficiency Half-Heusler Thermoelectric Materials for Energy Harvesting". Adv. Energy Mater. Vol. 5, (2015), 1500588 https://doi.org/10.1002/aenm.201500588

[15] W. G. Zeier, *et al.*, "Engineering half-Heusler thermoelectric materials using Zintl chemistry", Nat. Rev. Mater. Vol. 1 (2016), 16032 https://doi.org/10.1038/natrevmats.2016.32

[16] G. Joshi, *et al.*, "Enhancement in thermoelectric figure-of-merit of an n-Type half- heusler compound by the nanocomposite approach", *Adv. Energy Mater*., Vol. 1 (2011), p. 643–647 https://doi.org/10.1002/aenm.201100126

[17] S. Ballikaya *et al.*, "High thermoelectric performance of In, Yb, Ce multiple filled CoSb3 based skutterudite compounds", *Solid State Chem*., Vol. 193 (2012), p. 31-35 https://doi.org/10.1016/j.jssc.2012.03.029

[18] M. Mallick *et al*., "Thermophysical and magnetic properties of p- and n-type Ti-Ni-Sn based half-Heusler alloys", *J. Alloy. Compd*. Vol. 710 (2017), p. 191-198 https://doi.org/10.1016/j.jallcom.2017.03.268

[19] T. Zilber *et al.*, "TiNiSn half-Heusler crystals grown from metallic flux for thermoelectric applications", J. Alloy. Compd., Vol. 781 (2019), p. 1132-1138 https://doi.org/10.1016/j.jallcom.2018.12.165

[20] A. Berche *et al.*, "Oxidation of half-Heusler NiTiSn materials: Implications for thermoelectric applications", Intermetallics, Vol. 92 (2018), p. 62-71 https://doi.org/10.1016/j.intermet.2017.09.014